Quasi-two-dimensional acoustic metamaterial with negative bulk modulus

V. M. García-Chocano, R. Graciá-Salgado, D. Torrent, F. Cervera, and J. Sánchez-Dehesa*
Wave Phenomena Group, Universitat Politècnica de València, Camino de Vera s.n. (Edificio 7F), ES-46022 Valencia, Spain
(Received 22 December 2011; revised manuscript received 22 March 2012; published 14 May 2012)

We present the experimental realization and characterization of an acoustic metamaterial with negative bulk modulus. The metamaterial consists of a two-dimensional array of cylindrical cavities, and the bulk modulus is controlled by their radius size and length. Experiments are performed in a two-dimensional waveguide where a slab of seven layers is used to extract the parameters of the metamaterial. A complete characterization of the constructed structure is reported, including the dispersion relation of the acoustic bands and the skin depth effect, which both have been measured, and the data are well supported by semianalytical models and by finite-element simulations.

DOI: 10.1103/PhysRevB.85.184102 PACS number(s): 43.20.+g, 43.28.+h

I. INTRODUCTION

Acoustic metamaterials[1] or metafluids[2] are artificial structures consisting of subwavelength units with dynamical properties not available in natural materials. For example, acoustic metamaterials with negative inertial mass,[3–6] negative bulk modulus,[7–11] and both parameters simultaneously negative[12–14] have been reported in the last few years. It has been discussed that negative inertia is produced by dipolar resonances of the building units while negative bulk modulus is created by monopolar resonances.[12] Acoustic metamaterials with other extraordinary properties such as anisotropic inertia have been also proposed[15,16] and physically realized.[17,18] They are under research because of their potential applications such as as acoustic cloaks[19] or magnifying lenses.[20]

We are interested here in effective mediums with negative modulus. This property has been already studied using structures made of arrays of Helmholtz resonators[7,8,10,11] or by side holes in a narrow one-dimensional waveguide,[9] where they radiate like effective monopoles.

This work reports the physical realization of a quasi-two-dimensional (2D) metafluid with negative modulus. The metafluid consists of a 2D hexagonal lattice of cylindrical boreholes in a 2D waveguide. Note that the proposed structure is different from those previously reporting negative bulk modulus, which were mainly based on arrays of Helmholtz resonators[7,8,10,11] or side holes with both ends opened.[9,13] Moreover, the experimental characterization of the negativity of bulk modulus is here performed in a true 2D environment (a 2D waveguide) using a real 2D lattice of individual units. To the best of our knowledge, the reported works in this topic employed arrays of resonators characterized in a quasi-one-dimensional environment. The negative modulus in our proposed structure appears as a consequence of the interaction between the modes localized in the boreholes with the sound waves propagating inside the waveguide (WG). It is demonstrated that the artificial structure introduced is intrinsically low loss, is easily tunable, and has various interesting applications; the control of wave propagation inside waveguides is one of them.

The paper is organized as follows. After this introduction, in Sec. II the artificial structure defining the metafluid is introduced and the acoustic band structure of the periodic system is analyzed. In Sec. III a finite structure is constructed and experimentally characterized. The reflectance and transmittance spectra are measured and the effective parameters are extracted from them. Also, finite-element simulations are reported and compared with the experimental data. Section IV presents experiments showing that at the frequencies where the bulk modulus is negative, sound waves in the metamaterial exponential decay. The skin depth effect has been experimentally characterized and data are compared with an analytical model depending on the metafluid parameters. Finally, Sec. V summarizes the work performed.

II. THE TWO-DIMENSIONAL METAFLUID: ACOUSTIC BAND STRUCTURE

Let us consider an array of cylindrical boreholes with equal radii (R) and depths (L) drilled in a flat rigid surface. An acoustically rigid panel put on top, at a distance h from the surface, defines a 2D waveguide for sound propagation. Figure 1(a) depicts a scheme of the structure under study here. The underlying lattice is hexagonal with primitive lattice vectors $\mathbf{a}_1 = a(\frac{\sqrt{3}}{2}\hat{x} - \frac{1}{2}\hat{y})$ and $\mathbf{a}_2 = a(\frac{\sqrt{3}}{2}\hat{x} + \frac{1}{2}\hat{y})$, where a is the lattice period.

Recall that sound waves propagating in a 2D rigid-walled waveguide w have eigenfrequencies $\omega_{w,n} = 2\pi \times f_{w,n}$ that depend on the height h as follows:[21]

$$f_{w,n}^2(k_x,k_y) = \left(\frac{c}{2\pi}\right)^2 \left[k_x^2 + k_y^2 + \left(\frac{n\pi}{h}\right)^2\right], \qquad (1)$$

where c is the sound speed of air and n is an integer $n = 0, 1, 2, 3, \ldots$. Therefore, the wave number on the XY plane for the nth mode is given by the relation

$$k_{||,n} = \left[k_0^2 - \left(\frac{n\pi}{h}\right)^2\right]^{1/2}, \qquad (2)$$

where $k_0 = \omega/c$. Any particular mode n would propagate unattenuated if

$$k_0^2 - \left(\frac{n\pi}{h}\right)^2 > 0. \qquad (3)$$

First, we have studied how the frequency dispersion in Eq. (1) changes inside a WG having a hexagonal lattice of cylindrical boreholes drilled in the bottom surface. The solution has been

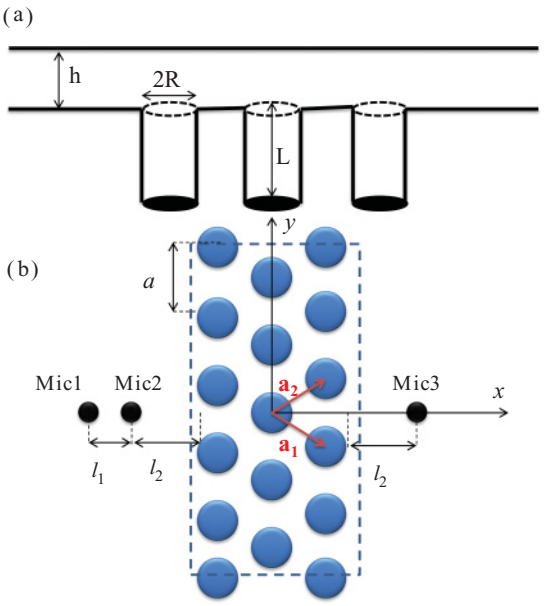

FIG. 1. (Color online) (a) Scheme of the metamaterial consisting of cylindrical boreholes in a two-dimensional waveguide of height h. (b) The experimental setup employed in its characterization. The blue circles represent the boreholes; $\mathbf{a}_1$ and $\mathbf{a}_2$ are the primitive vectors of the hexagonal lattice with parameter a. Three microphones (Mic) have been employed for measuring the transmittance and reflectance, the magnitudes needed for the parameters' extraction.

obtained by using the mode-matching technique[22] as explained below.

The pressure field in the waveguide, P_w, is obtained as a linear combination of Bloch modes satisfying the boundary conditions at the bottom and top surfaces. Since both surfaces of the WG are considered perfectly rigid, the normal component of the particle velocity, v_z, is zero at $z = 0$ (bottom surface) and at $z = h$ (top surface). The resulting expression for the pressure is

$$P_w(\boldsymbol{K},\boldsymbol{r},z;\omega) = \sum_{\boldsymbol{G}} A_{\boldsymbol{G}} e^{i\boldsymbol{K}\cdot\boldsymbol{r}} e^{i\boldsymbol{G}\cdot\boldsymbol{r}} \cos k_z(z-h) e^{i\omega t}, \quad (4)$$

where $\boldsymbol{r} = (x,y)$ defines an arbitrary point in the 2D space and $k_z^2 = k_0^2 - |\boldsymbol{K}+\boldsymbol{G}|^2$. The vectors of the reciprocal lattice are $\boldsymbol{G} = h_1\mathbf{b}_1 + h_2\mathbf{b}_2$, with $\mathbf{b}_1 = \frac{2\pi}{a}(\frac{1}{\sqrt{3}}\hat{x} - \hat{y})$ and $\mathbf{b}_2 = \frac{2\pi}{a}(\frac{1}{\sqrt{3}}\hat{x} + \hat{y})$. The vector $\boldsymbol{K} = \boldsymbol{K}(\omega)$ defines the dispersion relation of the acoustic band structure.

Inside the cylindrical holes, the pressure field P_h is obtained by making use of the method of separation of variables and the solution can be cast as follows:[21]

$$P_h(r,\theta,z;\omega) = \sum_{m=0}^{\infty}\sum_{n=1}^{\infty} J_m(k_{r,m,n}r) e^{im\theta} \times (B_1 e^{-ik_{0z}} + B_2 e^{+ik_{0z}}) e^{i\omega t}, \quad (5)$$

where (r,θ) are the polar coordinates in the XY plane, J_m are the Bessel function of order m, and $k_{r,m,n}$ denotes the discrete values that satisfy the equation corresponding to the condition that the radial velocity at the walls must be zero; i.e.,

$$\frac{dJ_m(k_r r)}{dr} = 0 \quad \text{at } r = R. \quad (6)$$

The value k_r corresponding to the nth root of this equation is $k_{r,m,n}$ and therefore

$$k_{z,m,n} = \left(k_0^2 - k_{r,m,n}^2\right)^{1/2}, \quad (7)$$

where the subindex m denotes the number of nodal lines passing through the center for transverse pressure distribution in a circular duct, and n gives the number of nodal lines with circular symmetry. With this notation, the plane mode has the (0,0) label and $k_{z,0,0} = k_0$. We have considered that this mode is the only one excited when a pressure with large wavelength (much larger than the hole diameter) is propagating along the 2D WG.

Therefore, the pressure field inside the holes is independent of the transversal coordinates and reduces to

$$P_h(z;\omega) = B_1 e^{-ik_{0z}} + B_2 e^{+ik_{0z}}, \quad (8)$$

where we have omitted the t dependence to simplify the notation. From here onward the dependence $e^{i\omega t}$ is implicitly assumed in all the equations. Since the normal velocity of the particle at the bottom surface must be zero, $\frac{\partial P_h}{\partial z} = 0$ at $z = -L$, the equation above becomes

$$P_h(z;\omega) = B\cos k_0(z+L). \quad (9)$$

Inside the 2D WG, the standard boundary conditions at the connecting (virtual) plane S between the waveguide and the holes are considered. First, the continuity of the pressure on the hole's surface $S = \pi R^2$ at $z = 0$ leads to

$$\sum_{\boldsymbol{G}} A_{\boldsymbol{G}} \cos k_z h \iint_S e^{i\boldsymbol{K}\cdot\boldsymbol{r}} e^{i\boldsymbol{G}\cdot\boldsymbol{r}} dS = \pi R^2 B \cos k_0 L, \quad (10)$$

where the surface integral can be easily evaluated,

$$\iint_S e^{i\boldsymbol{K}\cdot\boldsymbol{r}} e^{i\boldsymbol{G}\cdot\boldsymbol{r}} dS = 2\pi \frac{R}{|\boldsymbol{K}+\boldsymbol{G}|} J_1(|\boldsymbol{K}+\boldsymbol{G}|R). \quad (11)$$

Second, the continuity of the normal component of particle velocity through the unit cell's surface S_d gives

$$k_z A_{\boldsymbol{G}} S_d \sin k_z h = -k_0 B \sin k_0 L \iint_S e^{-i\boldsymbol{K}\cdot\boldsymbol{r}} e^{-i\boldsymbol{G}\cdot\boldsymbol{r}} dS. \quad (12)$$

From these equations and after easy manipulations we arrive at the equation describing the band structure,

$$\cot \omega L/c = f\chi(\omega,\boldsymbol{K}), \quad (13)$$

where f denotes the lattice filling fraction, $f = S/S_d$, and

$$\chi(\omega,\boldsymbol{K}) = -4\sum_{\boldsymbol{G}} \frac{k_0 \cos k_z h}{k_z \sin k_z h} \left(\frac{J_1(|\boldsymbol{G}+\boldsymbol{K}|R)}{|\boldsymbol{G}+\boldsymbol{K}|R}\right)^2. \quad (14)$$

Figure 2 shows the calculated dispersion relation of the propagating modes in a WG for three h values: $h/a = 1.667$ (a), $h/a = 0.5$ (b), and $h/a = 0.1$ (c). The radius and depth of the boreholes are $R = a/3$ and $L = 3a$, respectively, and they are fixed parameters. Again, let us remark that results are obtained by using only the fundamental mode in the cylindrical holes [see Eq. (9)]. This approach is reasonable in the low-frequency region, where the wavelengths are large in comparison with the hole diameter.

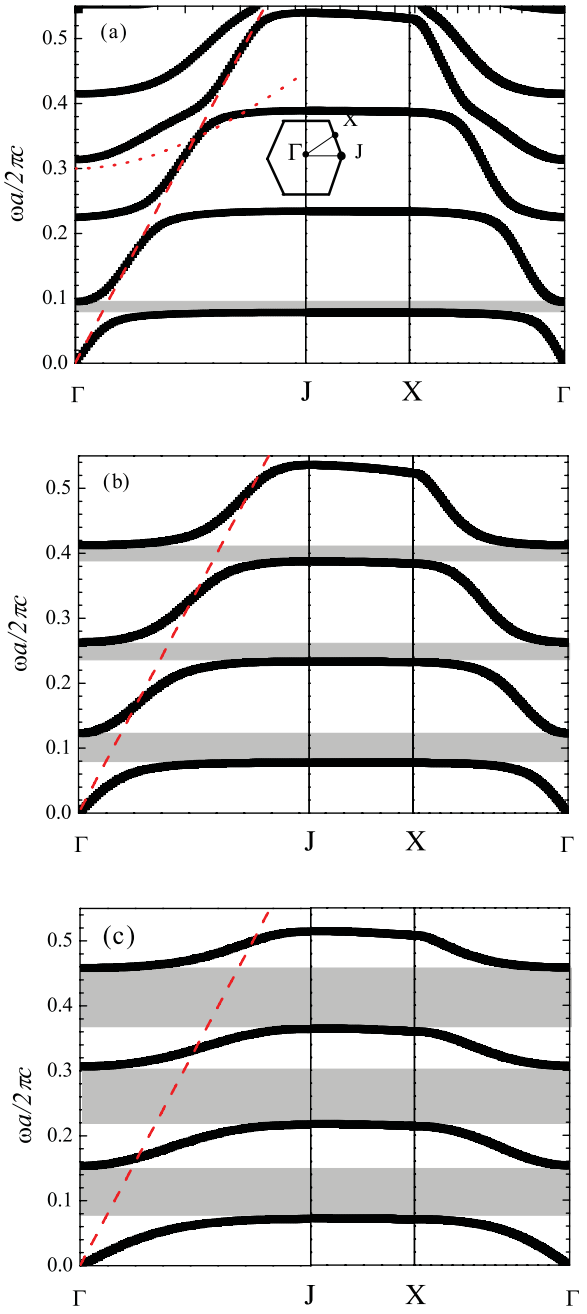

FIG. 2. (Color online) The band structure of the acoustic metamaterial consisting of a two-dimensional array of cylindrical boreholes with hexagonal symmetry and lattice constant a (see Fig. 1). The bands are depicted for three different waveguide heights: (a) $h = 1.667a$, (b) $h = 0.5a$, and (c) $h = 0.1a$. The radius and depth of boreholes are $R = 0.3a$ and $L = 3a$, respectively. The dashed (dotted) lines give the dispersion relation of the fundamental $n = 0$ (first excited, $n = 1$) mode propagating in the waveguide without boreholes. The inset shows the Brillouin zone of the hexagonal lattice and its high-symmetry points.

At this point, let us recall that the linear frequency of the resonances localized in a cylindrical borehole b with length L and radius R are (in reduced units)[21]

$$\overline{f}_{b,m} \equiv \frac{\omega_{b,m}a}{2\pi c} = \frac{m}{4\left(\frac{L}{a} + 0.8\frac{R}{a}\right)}, \qquad (15)$$

where m is an odd number (1, 3, 5,. . .). For the holes employed in this study, the corresponding frequencies are $\overline{f}_{b,1} = 0.076$, $\overline{f}_{b,3} = 0.229$, and $\overline{f}_{b,5} = 0.383$, which correspond to the flat bands shown in Figs. 2(a)–2(c).

The thick continuous lines in Fig. 2 represent the acoustic bands, which are plotted along the high-symmetry directions in the Brillouin zone (BZ) of the hexagonal lattice (see the inset), where $k_J = 2\pi/a(2/3,0)$. The dashed and dotted lines represent the dispersion relation of modes $f_{w,0}$ and $f_{w,1}$, respectively, in the empty 2D WG [see Eq. (1)].

$$\overline{f}_{w,0}(k_x,k_y) \equiv \frac{f_{b,0}a}{2\pi c} = \frac{a}{2\pi}\left[k_x^2 + k_y^2\right]^{1/2},$$
$$\overline{f}_{w,1}(k_x,k_y) \equiv \frac{f_{b,1}a}{2\pi c} = \frac{a}{2\pi}\left[k_x^2 + k_y^2 + \left(\frac{\pi}{h}\right)^2\right]^{1/2}. \qquad (16)$$

Note that the first excited band at the Γ point takes the value $\overline{f}_{w,1}(0,0) = (a/2h) = 0.30$ for $h = 1.667a$ and the dotted line in Fig. 2(a) represents the full dispersion relation. However, the bands corresponding to values $h = 0.5a$ and $h = 0.1a$ have frequencies above the region represented in Figs. 2(b) and 2(c), respectively. It is observed that the dispersion relation of frequencies propagating inside the WG with holes are the result of the interaction between the modes localized within the holes (the flat bands) with the modes propagating in the empty waveguide.

Figure 2(a) shows that the interaction between the first borehole mode $\overline{f}_{b,1}$, with the fundamental mode $\overline{f}_{w,0}$ of the WG producing a complete band gap in the region [0.078–0.095]. This band gap appears at frequencies much lower than that of the Bragg band gap with midgap at about $\overline{f}_{\text{Bragg}} \approx k_J a/2\pi = 0.667$ (not shown in Fig. 2).

The existence of low-frequency gaps in the dispersion relation of phononic crystals is typically associated with the existence of low-frequency modes in the individual scatterers and have been extensively described in the literature.[3,5,7,8] For example, the analysis reported by Wang and coworkers[8] on the band structure of a narrow one-dimensional (1D) WG with a periodic array of Helmholtz resonators leads to similar conclusions; i.e., the interaction between the resonant modes with the propagating waves produces a band gap opening around the resonant frequencies. In our case the low-frequency band gap is determined by the borehole resonances that can be easily tuned by changing the parameters L and R.

Figures 2(b) and 2(c) show that narrowing the WG (i.e., decreasing h) produces an enhancement of the interaction between the waves propagating in the WG with the 1D modes localized in the holes. From these figures one can conclude that for $h \to 0$ the dispersion relation will consist of a lowest band starting from zero at the Γ point and that reaches the frequency value $\bar{f}_{b,1}$ in Eq. (15). For frequencies above $\bar{f}_{b,1}$, we will obtain a set of dispersionless bands corresponding to the discrete levels $m = 2, 3, 4, \ldots$ in Eq. (15).

III. EXPERIMENTAL CHARACTERIZATION

To support the previous findings we have constructed a sample consisting of seven rows of hollow brass cylinders with length $L = 9$ cm and radius $R = 1$ cm. Each row contains 15 cylinders along the y axis. They were attached to a Plexiglass

plate with area 68 cm × 68 cm where a hexagonal lattice (with lattice constant $a = 3$ cm) had been drilled. The sample was placed at the center of a 2D acoustic waveguide with dimensions 460 cm × 366 cm × 5 cm, the height being $h =$ 5 cm in Fig. 1(a). The top surface of the WG was constructed with a wooden panel and we used the floor of the room as the WG bottom surface. The temperature inside the WG during the measurements takes a value 23.7 ± 0.1 °C, which gives a sound speed with a practically constant value $c = 345$ m/sec, which has been used in the numerical simulations.

It is worth noting that modes with variations along the vertical direction (z axis in Fig. 1) are not expected until frequencies above the cutoff of $\omega_{w,1}(0,0) = 2\pi \times 3.45$ kHz, which corresponds to the condition when h equals a half wavelength. The sound propagating inside the WG is excited using a column speaker placed at the front of the WG. The laterals are covered by a 5-cm-thickness layer of fiberglass to avoid undesired reflections. At the opposite face of the speaker there is a programmable robot that moves a microphone with spatial resolution of 5 mm along a line under the sample in order to measure the profile of the pressure along the air/metamaterial interface, which is discussed in Sec. IV.

Excitation data are generated by a NI PCI-6731 card. The analog output of this device goes to a power amplifier that drives the column speaker. It is worth noting that some reflections take place between the speaker, the room, and the open faces of the 2D waveguide. Because of this, a time-limited signal is emitted and then the data are acquired until the arrival time of the first unwanted reflection. Thus, the measurements are performed under echo-free conditions. The excitation signal consists of a sine wave modulated by a Gaussian envelope. The frequency of the carrier is 2.5 kHz and the spectrum of the whole signal covers a frequency range from the low-frequency cutoff of the speaker (around 80 Hz) up to 5 kHz.

The scattered sound by the sample is recorded by three B&K 4958 microphones Mic1, Mic2, and Mic3, put at fixed locations on the sample holder, as is schematically depicted in Fig. 1(b) with $l_1 = 3$ cm and $l_2 = 9$ cm. The data received by the microphones is amplified by a B&K 2694-B device. The resulting signal is then acquired by a PicoScope 3224 digitizer which loads the data into a computer. During the measurement, one pulse is emitted and all the frequency components are obtained from the acquired data through a fast Fourier transform. In order to reduce the presence of random noise, several pulses are emitted and their responses are averaged. This process is performed once for the microphones placed at the fixed locations of Fig. 1(b) and also at each position of the spatial sweep under the sample. All the procedure (sound generation, robot motion, sound reception, and processing) is managed by a custom homemade program.

A. Acoustic bands

The seven layers of the structure under study are aligned along the ΓJ direction of the BZ and its total width is taken as $D = 7 \times \frac{\sqrt{3}}{2} a = 21.87$ cm, which has been calculated by considering that the surfaces are located at a half distance of the layer separation. This is a custom assumption when working with crystalline structures terminating in a surface.

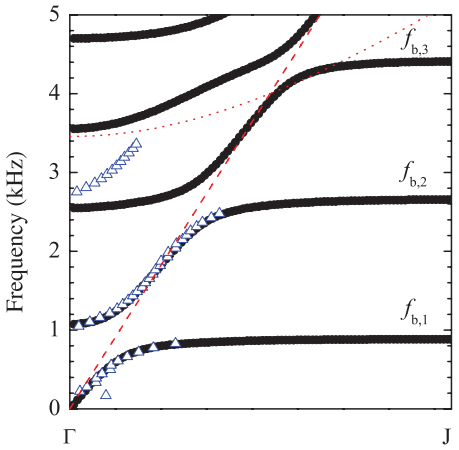

FIG. 3. (Color online) Acoustic band structure along the high-symmetry direction ΓJ of the Brillouin zone. The symbols represent the bands measured using a phase-shift technique. The black lines are the calculated dispersion relation using a mode-matching technique. They correspond (in kHz) to those shown in Fig. 2(a). The dashed (dotted) line defines the dispersion relation of mode 0 (1) in the free waveguide [see Eq. (1)].

The sample thickness D is large enough so that the dispersion relation can be derived experimentally from the phase of the transmission coefficient φ_T through the relation $\varphi_T = k_s D + 2\pi\ell$, where ℓ is an integer and k_s is the wave number of the sample to be calculated. Band gaps in the dispersion relation are identified by discontinuities in φ_T, so after this effect the parameter ℓ must be modified in order to place correctly the next band.

The symbols in Fig. 3 represent the points experimentally measured using this technique. Note the general good agreement between the measured dispersion relation and that predicted by our modeling. However, it is observed that for frequencies around 3 kHz the agreement between theory and data is not good enough, probably due to the fact that the condition of homogenization is not perfectly accomplished as it is shown below.

B. Reflectance and transmittance spectra

For low frequencies, which is the region of interest in this work, the sound propagates with a plane wave front and the pressure field along the axis of propagation can be obtained by solving the wave equation for 1D propagation,

$$\frac{d}{dx}\left[\frac{1}{\rho(x;\omega)}\frac{dP(x;\omega)}{dx}\right] + \frac{\omega^2}{B(x;\omega)}P(x;\omega) = 0, \qquad (17)$$

where parameters $\rho(x;\omega)$ and $B(x;\omega)$ are inhomogeneous and might be frequency dependent.

Within the WG, we can distinguish two regions that we associate with mediums I and II, which correspond to the air in the WG without and with boreholes, respectively. For medium I, the wave equation reduces to

$$\frac{1}{\rho_0}\frac{d^2P^I(x;\omega)}{dx^2} + \frac{\omega^2}{B_0}P^I(x;\omega) = 0, \qquad (18)$$

where $B_0 = 1.01 \times 10^5$ Pa and $\rho_0 = 1.2041$ Kg/m^3 are the modulus and density of air.

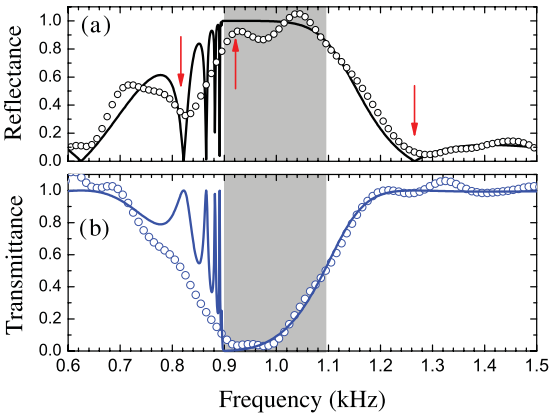

FIG. 4. (Color online) (a) Reflectance of a sample consisting of seven rows of hollow metallic tubes opened to a two-dimensional waveguide with height $h = 5$ cm [see Fig. 1(a)]. The tubes are arranged in a hexagonal configuration with lattice parameter $a = 3$ cm and have dimensions $L = 9$ cm and $R = 1$ cm. (b) The corresponding transmittance. The symbols in both plots are the measured data while the continuous lines represents the simulations using finite elements.

The reflection coefficient r is rapidly obtained by using the data recorded by Mic1 and Mic2 embedded in the formula resulting from 1D propagation,[23]

$$\mathsf{r} = \frac{P_2 e^{-ik_0 x_1} - P_1 e^{-ik_0 x_2}}{P_1 e^{ik_0 x_2} - P_2 e^{ik_0 x_1}}, \tag{19}$$

where P_1 and P_2 are the complex values of pressure taken at the positions x_1 and x_2 of microphones Mic1 and Mic2, respectively. Note that Eq. (19) is not valid when $x_2 - x_1$ equals an integer multiple of a half wavelength, setting an upper frequency limit to the measures. Since Mic1 and Mic2 are separated by $l_1 = 3$ cm, this limit is therefore located at 5750 Hz, which is higher than the frequencies of interest.

The symbols in Fig. 4(a) give the reflectance spectrum obtained from the data recorded and the expression in Eq. (19). The continuous lines represent the finite-element simulations using the same experimental setup. Note that simulations give interesting features in the spectrum, such as the narrow deeps associated with Fabry-Perot-like modes, which are above the accuracy limit of our experimental setup. The experimental profiles present the main spectral features predicted by finite-element simulations in spite of the simple method [see Eq. (19)] employed in its derivation.

The transmittance is obtained by recording data in Mic2 and Mic3 and the expression[23]

$$T(\omega) = \frac{P_3}{P_2} \frac{e^{-ik_0 x_2} + \mathsf{r} e^{ik_0 x_2}}{e^{-ik_0 x_3}} e^{-ik_0 d}, \tag{20}$$

where P_3 is the pressure measured by Mic3 at position x_3, and d is the sample thickness. The transmittance spectrum is depicted in Fig. 4(b) together with the corresponding numerical simulations. As in the case of the reflectance spectrum, a general good agreement is found between transmittance data and finite element simulations.

For the sake of comprehensiveness, we report in Fig. 5 and Fig. 6 the maps of the pressure amplitude calculated by finite

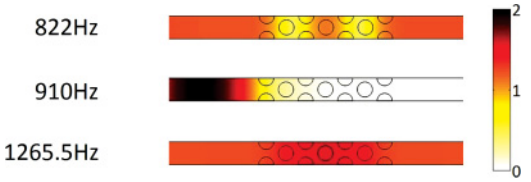

FIG. 5. (Color online) Map of the pressure amplitude taken at the equatorial plane of the two-dimensional waveguide shown in Fig. 1. The selected frequencies are denoted by arrows in Fig. 4.

elements. The selected frequencies correspond to spectral features in the reflectance spectrum shown in Fig. 4(a). The lowest frequency, 822 Hz, corresponds to a Fabry-Perot-like resonance, which is characterized by a dip (peak) in the reflectance (transmittance) spectrum. The 2D map in Fig. 5 clearly show its physical behavior, where a wavelength perfectly matches the sample thickness, D. Inside the cylindrical cavities, Fig. 6(a) shows a huge sound localization, the sound intensity being dependent on the cavity position along the x axis; the highest are obtained at the first, middle, and last rows, which correspond to maximum amplitude in the equatorial plane (see Fig. 5). For the frequency 910 Hz, which belongs to the band gap, the corresponding map in Fig. 5 shows the perfectly reflecting behavior and the first row of cylinders is the only one where sound penetrates, as seen in Fig. 6(b). Finally, for the frequency above the band gap, 1265.5 Hz, Fig. 5 shows a perfect transmission of sound and Fig. 6(c) demonstrates that

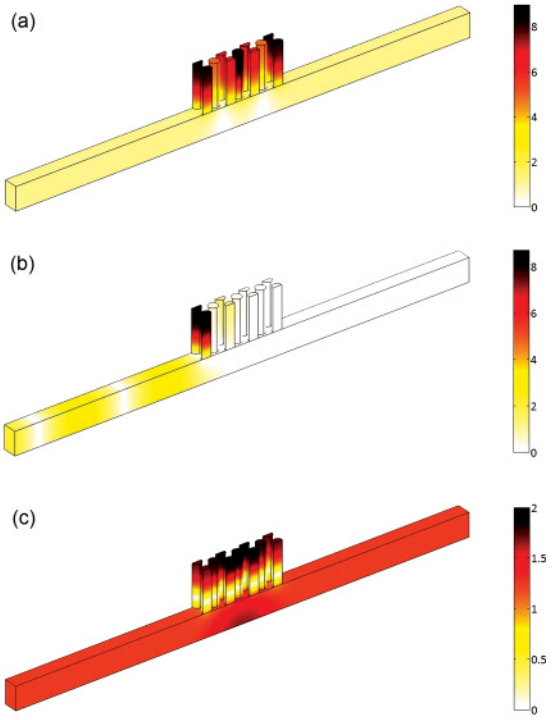

FIG. 6. (Color online) Maps of the pressure amplitudes inside the artificial structure under study. They are obtained by finite-element simulation at three selected frequencies, which are denoted by arrows in Fig. 4: (a) 822 Hz, (b) 910 Hz, and (c) 1265.5 Hz.

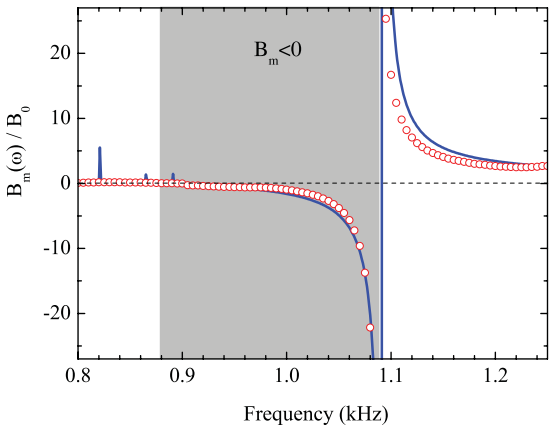

FIG. 7. (Color online) The frequency-dependent effective bulk modulus of the metamaterial. The symbols represent the modulus derived from the reflectance and transmittance spectra while the continuous line defines the extracted parameter from finite-element simulations.

sound penetrates in all the cavities that have the same intensity profiles along the cylindrical axis.

C. Effective parameters

We are interested in the properties of the structure at frequencies below a certain frequency cutoff defining the homogenization limit. It has been experimentally established[25] that the frequency cutoff is $\omega_c = 2\pi \times c/4a$ for the case of hexagonal arrays of rigid cylinders in air. We employ this limit, which takes the value $\omega_c = 2\pi \times 2.87$ kHz for the structure under study, since its validity has been demonstrated in many equivalent structures consisting of sonic scatterers in air background. Therefore, the artificial structure studied acts as a true acoustic metamaterial with given effective parameters, whose values are extracted below, for any linear frequency under 2.87 kHz.

The frequency-dependent effective parameters of the metamaterial $\rho_m(\omega)$ and $B_m(\omega)$ are derived using the data of $R(\omega)$ and $T(\omega)$ and the procedure explained in Ref. 24. The extracted effective mass density does not depend on the frequency and its value is practically equal to that of the background ρ_0. The extracted effective bulk modulus, $B_m(\omega)$, normalized to that of air, is depicted by symbols in Fig. 7, where the shadowed region indicated the frequencies at which the bulk modulus takes negative values.

The effective parameters have been also extracted by using the reflectance and transmittance spectra obtained from finite-element simulations and the expressions in Ref. 24. Figure 7 depicts the theoretically extracted bulk modulus (continuous line) and its comparison with the values derived from experimental data (symbols). A good agreement is observed between theory and experiments. Note that the bulk modulus is negative in the frequency region coincident with the first band gap, which is defined by the gray region. The extracted effective mass density is practically a constant function with value $\rho_m \cong 0.98\rho_0$.

We conclude that the artificial structure under study behaves as an effective medium that has a bulk modulus $B_m(\omega)$ with profile similar to that reported for the case of array of Helmholtz resonators, and can be expressed in the form

$$B_m^{-1} = B_0^{-1}\left[1 - \frac{F\omega_0^2}{\omega^2 - \omega_0^2 + i\Gamma\omega}\right], \tag{21}$$

where F is a factor defining the band gap width, which is determined by the frequencies $\omega_0 < \omega < \omega_0\sqrt{1+F}$, ω_0 is the resonant angular frequency, and Γ is the dissipation loss in the resonating boreholes. The profile shown in Fig. 7 fits perfectly this Fano-like profile by using the values $\omega_0 = 2\pi \times 874$ Hz, which is the frequency of the mode $m = 1$ of the closed tube, and $F = 0.556$, which determines the band gap width. The loss term ($\Gamma = 2\pi \times 3.4$ Hz) is the only fitted parameter and its value is much lower than that reported ($\Gamma = 2\pi \times 400$ Hz) for negative modulus metamaterials based on arrays of Helmholtz resonators.[7] The losses in our structure are also lower than that measured with one-dimensional arrays of side holes, a structure that has been presented as low loss metamaterial with negative modulus.[9]

It is important to point out that our proposed structures have lower losses than those previously reported due to different reasons. On the one hand, in comparison with those based on Helmholtz resonators,[7,8,10,11] our structures do not present narrow channels where strong energy dissipation is expected due to friction with the walls. On the other hand, in comparison with the structures consisting of side holes,[9,13] our structures do not present radiative losses since the ends of the holes are closed.

IV. THE SKIN-DEPTH EFFECT AT THE AIR/METAMATERIAL INTERFACE

Let us consider now the simple case in which we have a interface between two semi-infinite mediums: Medium I is the air with positive mass and modulus, whereas medium II is the metamaterial under study with positive mass ρ_m and negative bulk modulus B_m. Hence, Eq. (17) particularized to the metamaterial (medium II), which is defined in the region $x \geqslant 0$, becomes

$$\frac{1}{\rho_m}\frac{d^2P^{II}(x;\omega)}{dx^2} - \frac{\omega^2}{|B_m(x;\omega)|}P^{II}(x;\omega) = 0. \tag{22}$$

The solution of this equation is

$$P^{II}(x;\omega) = P_0 e^{-x/\delta}, \tag{23}$$

where P_0 denotes the pressure amplitude at $x = 0$, the air/metamaterial interface, and δ defines the skin-depth of the metamaterial, whose expression is quickly obtained by substitution of Eq. (23) in Eq. (22),

$$\delta^2 = \frac{1}{\omega^2}\frac{|B_m(\omega)|}{\rho_m}. \tag{24}$$

The wave equation for sound propagation in air (medium I) is given by Eq. (18) and its solution is

$$P^I(x;\omega) = e^{ik_0x} + \mathsf{r}e^{-ik_0x}, \tag{25}$$

where r is here the reflection coefficient.

The coefficient r is determined by applying the continuity of the pressure and normal velocity at the air/metamaterial

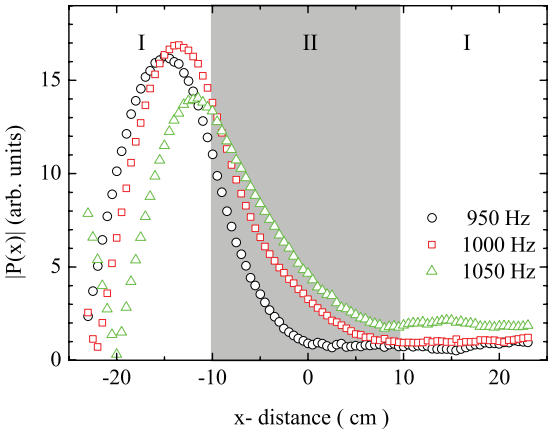

FIG. 8. (Color online) Pressure amplitude measured along the x axis of a metamaterial slab made of seven layers of cylindrical holes. The exponential decay is observed inside the metamaterial slab (light-gray region).

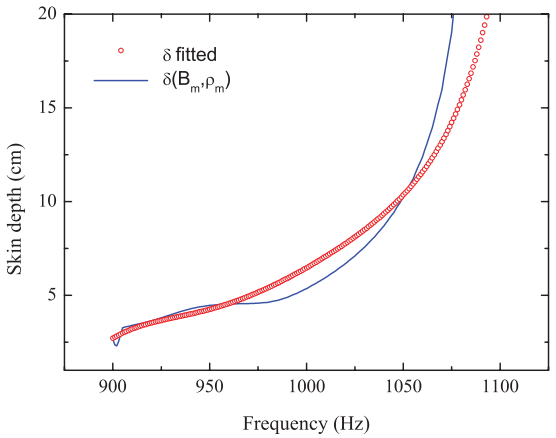

FIG. 9. (Color online) The skin depth δ as a function of the frequency. The symbols represent the values obtained by adjusting the amplitude profiles shown in Fig. 8 to the function exponentially decreasing shown in Eq. (23). The continuous lines are the values predicted by the model in Eq. (24) in which we have employed the parameters derived from experiments.

interface. After easy algebra its expression can be cast as

$$\mathsf{r} = -\frac{Z_0 - i\,Z_m(\omega)}{Z_0 + i\,Z_m(\omega)}, \tag{26}$$

where $Z_0 = \sqrt{B_0\rho_0}$ and $Z_m(\omega) = \sqrt{|B_m(\omega)|\rho_m}$ are the characteristic impedances of air and metamaterial, respectively.

The expression for r indicates that the reflectance $\mathsf{R}(\omega) = |\mathsf{r}|^2 = 1$ (total reflection) for any frequency. The reflectance spectrum shown in Fig. 4(a), which has been taken for a finite metamaterial sample, shows that this conclusion is true for a wide frequency region within the band gap. We use this result to analyze the wave transmission-reflection at the interface by using the simple formulas obtained from the two semi-infinite mediums.

Experimentally, we have employed a microphone to scan the 2D WG along the x axis. Figure 8 depicts the pressure amplitude as a function of the position for three different frequencies inside the band gap. It is observed that the field impinging the metamaterial is an oscillating function while inside the metamaterial is a function exponentially decreasing.

The skin depth δ has been experimentally determined by adjusting the profiles in Fig. 8 to an exponential decaying function. The resulting values are depicted by symbols in Fig. 9 and are compared with those (continuous line) obtained using the formula given by Eq. (24). It can be concluded that δ increases monotonously in the region where the reflectance is unity. For frequencies approaching the resonance of $B_m(\omega)$, the skin depth increases with frequency following an exponential profile.

V. SUMMARY

In summary, we have introduced an intrinsically low loss quasi-two-dimensional acoustic metamaterial with negative bulk modulus. The artificial structure consists of a 2D periodic distribution of cylindrical boreholes opened to a 2D waveguide. Measurements and an analytical model demonstrate that the region of negative modulus develops an acoustic band gap whose width is tunable with the geometrical parameters of boreholes (radius and length). A complete characterization of a sample has been reported including the skin-depth effect. It can be concluded that this metamaterial can be used to filter the sound propagating in waveguides with high efficiency. On the other hand, the extraordinary sound amplitude obtained inside the hole cavities can be used to design highly absorbing devices by filling up the holes with dissipative materials.

Starting from the structure reported here, a double negative metamaterial can be easily achieved by adding a lattice of membranes as described in Ref. 6. Finally, let us remark that these results can be extended to waveguides consisting of the boreholes filled with water and a water film on top. The resulting structure will also show interesting properties in order to control and guide underwater sound.

ACKNOWLEDGMENTS

This work was supported by the Spanish MICINN under Contracts No. TEC2010-19751 and No. CSD2008-0066 (CONSOLIDER program), and by the USA Office of Naval Research. We acknowledge the technical help by A. Díaz-Rubio and A. Climente. J.S.-D. acknowledges useful discussions with A. Broatch and A. Krokhin. D.T. acknowledges the postdoctoral grant provided by the UPV under the program *Campus de excelencia internacional*.

*jsdehesa@upvnet.upv.es

[1] L. Fok, M. Ambati, and X. Zhang, MRS Bull. **33**, 931 (2008).

[2] A. N. Norris, J. Acoust. Soc. Am. **125**, 839 (2009).

[3] Z. Liu, X. Zhang, Y. Mao, Y. Zhu, Z. Yang, C. T. Chan, and P. Sheng, Science **289**, 1734 (2000).

[4]Z. Yang, J. Mei, M. Yang, N. H. Chan, and P. Sheng, Phys. Rev. Lett. **101**, 204301 (2008).
[5]S. Yao, X. Zhou, and G. Hu, New J. Phys. **10**, 043020 (2008).
[6]C. M. Park, J. J. Park, S. H. Lee, Y. M. Seo, C. K. Kim, and S. H. Lee, Phys. Rev. Lett. **107**, 194301 (2011).
[7]N. Fang, D. Xi, J. Xu, M. Ambati, W. Srituravanich, C. Sun, and X. Zhang, Nature Mater. **5**, 452 (2006).
[8]Z. G. Wang, S. H. Lee, C. K. Kim, C. M. Park, K. Nahm, and S. A. Nikitov, J. Appl. Phys. **103**, 064907 (2008).
[9]S. H. Lee, C. M. Park, Y. M. Seo, Z. G. Wang, and C. K. Kim, J. Phys.: Condens. Matter **21**, 17504 (2009).
[10]C. Ding, L. Hao, and X. Zhao, J. Appl. Phys. **108**, 074911 (2010).
[11]J. Fey and W. M. Robertson, J. Appl. Phys. **109**, 114903 (2011).
[12]J. Li and C. T. Chan, Phys. Rev. E **70**, 055602(R) (2004).
[13]S. H. Lee, C. M. Park, Y. M. Seo, Z. G. Wang, and C. K. Kim, Phys. Rev. Lett. **104**, 054301 (2010).
[14]D. Torrent and J. Sánchez-Dehesa, New J. Phys. **13**, 093018 (2011).
[15]D. Torrent and J. Sánchez-Dehesa, New J. Phys. **10**, 023004 (2008).
[16]J. B. Pendry and J. Li, New J. Phys. **10**, 115032 (2008).
[17]D. Torrent and J. Sánchez-Dehesa, Phys. Rev. Lett. **105**, 174301 (2010).
[18]I. Spiousas, D. Torrent, and J. Sánchez-Dehesa, Appl. Phys. Lett. **98**, 244102 (2011).
[19]S. A. Cummer and D. Schurig, New J. Phys. **10**, 023004 (2007).
[20]J. Li, L. Fok, X. Yin, G. Bartal, and X. Zhang, Nature Mater. **8**, 931 (2009).
[21]M. L. Munjal, *Acoustics of Ducts and Mufflers* (Wiley, New York, 1987).
[22]R. E. Collin, *Field Theory of Guided Waves* (IEEE, New York, 1996), p. 287.
[23]D. H. Towne, *Wave Phenomena* (Dover, New York, 1967).
[24]V. Fokin, M. Ambati, C. Sun, and X. Zhang, Phys. Rev. B **76**, 144302 (2007).
[25]D. Torrent, A. Håkansson, F. Cervera, and J. Sánchez-Dehesa, Phys. Rev. Lett. **96**, 204302 (2006).